PLOS ONE

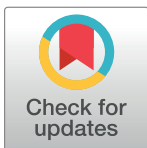# Disruption of *Osteoprotegerin* has complex effects on medial destruction and adventitial fibrosis during mouse abdominal aortic aneurysm formation

Batmunkh Bumdelger☯, Mikage Otani☯, Kohei Karasaki, Chiemi Sakai, Mari Ishida, Hiroki Kokubo📷*, Masao Yoshizumi*

Department of Cardiovascular Physiology and Medicine, Graduate School of Biomedical and Health Sciences, Hiroshima University, Hiroshima, Japan

☯ These authors contributed equally to this work.
* hkokubo@hiroshima-u.ac.jp (HK); yoshizum-tky@umin.ac.jp (MY)

Abstract

Aortic aneurysm refers to dilatation of the aorta due to loss of elasticity and degenerative weakening of its wall. A preventive role for osteoprotegerin (Opg) in the development of abdominal aortic aneurysm has been reported in the $CaCl_2$-induced aneurysm model, whereas Opg was found to promote suprarenal aortic aneurysm in the AngII-induced *ApoE* knockout mouse aneurysm model. To determine whether there is a common underlying mechanism to explain the impact of Opg deficiency on the vascular structure of the two aneurysm models, we analyzed suprarenal aortic tissue of 6-month-old $ApoE^{-/-}Opg^{-/-}$ mice after AngII infusion for 28 days. Less aortic dissection and aortic lumen dilatation, more adventitial thickening, and higher expression of collagen I and Trail were observed in $ApoE^{-/-}Opg^{-/-}$ mice relative to $ApoE^{-/-}Opg^{+/+}$ mice. An accumulation of α-smooth muscle actin and vimentin double-positive myofibroblasts was noted in the thickened adventitia of $ApoE^{-/-}Opg^{-/-}$ mice. Our results suggest that fibrotic remodeling of the aorta induced by myo-fibroblast accumulation might be an important pathological event which tends to limit AngII-induced aortic dilatation in $ApoE^{-/-}Opg^{-/-}$ mice.

Introduction

Aortic aneurysm (AA) refers to a dilatation of the aorta due to loss of elasticity and degenerative weakening of its wall. Continuous expansion of the aorta results in rupture and is associated with a high mortality rate [1]. Analyses of AA in experimental animal models, including the $CaCl_2$-induced mouse model and the AngII-induced *ApoE* knockout (KO) mouse model [2, 3], are important for understanding the pathogenesis of this disease and for developing effective drug treatments aimed at arresting aortic expansion [4–7].

Osteoprotegerin (Opg, also referred to as TNFRSF11B), a member of the tumor necrosis factor (TNF) receptor superfamily, functions as a decoy receptor to regulate various factors

across many biological processes [8]. For example, Opg has been shown to regulate bone metabolism through the Receptor activator of nuclear factor kappa-B ligand (Rankl) [9, 10] and apoptosis of cancer cells through TNF-related apoptosis-inducing ligand (Trail). Given that vascular diseases are often involved in bone pathologies [11, 12], and because Opg is expressed in vascular smooth muscle cells (VSMCs) [13] and serum levels of OPG are elevated in cardiovascular disease [14–17], there is great interest in the roles Opg may play in the vascular system.

We recently reported that Opg plays a preventive role in the development of abdominal AA (AAA) in the CaCl$_2$-induced aneurysm model [18]. In *Opg* KO mice, we found larger aneurysms with destruction of the aortic medial layer, which had increased expression of matrix metalloproteinase (Mmp)-9 and Trail. The expression of Opg in aortic tissue was also increased in response to aneurysm induction in wild-type mice. We concluded in this recent study that Opg prevents AAA formation through its antagonistic effect on Trail. However, another group reported that Opg can promote the development of aneurysms in the suprarenal aorta (SRA) in the AngII-induced *ApoE* KO mouse model [19]. The authors of that study attributed the lower incidence of aneurysms and rupture in *ApoE$^{-/-}$Opg$^{-/-}$* mice to the downregulation of proteolytic enzyme expression. The two reports discussed above suggest opposing results for aneurysm formation in *Opg*-deficient mice. Interestingly, a recent study found that low dose Opg had a preventive effect in both AAA models, although the mechanism underlying the preventive effect is unclear [20].

In the present study, we found a lower incidence of aortic dissection and a lower tendency for aortic dilatation in *Opg*-deficient mice. There were no structural differences in medial elastic fibers between *ApoE$^{-/-}$Opg$^{-/-}$* and *ApoE$^{-/-}$Opg$^{+/+}$* mice. However, more adventitial thickening and increased expression of collagen I, α-smooth muscle actin (SMA), vimentin, and Trail were observed in *ApoE$^{-/-}$Opg$^{-/-}$* mice relative to *ApoE$^{-/-}$Opg$^{+/+}$* mice. This suggests that fibrotic remodeling of the aorta may have resulted from an accumulation of myofibroblasts in *ApoE$^{-/-}$Opg$^{-/-}$* mice, which was also previously observed in the CaCl$_2$-induced AAA model [18]. Our results suggest that Opg deficiency may lead to fibrotic remodeling of the aorta, possibly enhanced by Trail signaling, and is an important pathological event that tends to limit AngII-induced SRA dilatation and dissection in *ApoE* KO mice.

Results

Opg deficiency tends to limit AngII-induced aortic dissection and dilatation

In order to confirm the phenotypic differences in the two aneurysm models resulting from *Opg* deficiency, we crossed *Opg* KO mice with *ApoE* KO mice to generate *ApoE$^{-/-}$Opg$^{-/-}$* mice. The *Opg* KO mice were then treated with AngII to promote aneurysm development in the suprarenal aorta (SRA) (S1A Fig in S1 File). Although Moran et al. reported a significantly smaller median maximum diameter of the SRA in *ApoE$^{-/-}$Opg$^{-/-}$* mice compared to that in *ApoE$^{-/-}$Opg$^{+/+}$* mice, we did not observe a significant reduction in the maximum external diameter in *ApoE$^{-/-}$Opg$^{-/-}$* mice relative to *ApoE$^{-/-}$Opg$^{+/+}$* mice (Fig 1A and 1B, S2A Fig–S2C Fig in S1 File). Moreover, no significant differences were observed in survival rate and concentrations of serum cholesterol between *ApoE$^{-/-}$Opg$^{-/-}$* and *ApoE$^{-/-}$Opg$^{+/+}$* mice at 28 days after AngII infusion (S2F Fig and S2G Fig in S1 File). However, on visual inspection, the diameter of the SRA in *ApoE$^{-/-}$Opg$^{-/-}$* mice appeared to be somewhat smaller, and multiple hematomas were observed in the SRA of *ApoE$^{-/-}$Opg$^{+/+}$* mice. Thus, we adopted Daugherty's classification system for aortic aneurysms [21] and categorized the mice into three groups based on dilatation of the SRA and the presence of visible hematoma (No Aneurysm, Aneurysm, and
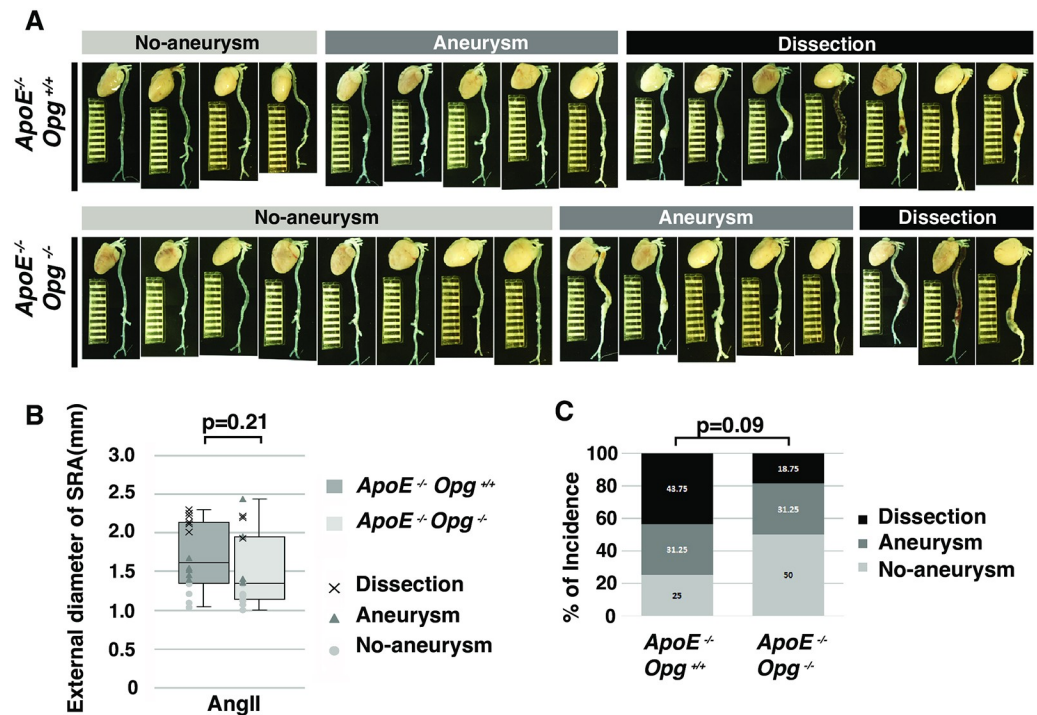
Fig 1. Opg deficiency tends to suppress AngII-induced aortic aneurysms. (A) Aortas of AngII-infused *ApoE*$^{-/-}$*Opg*$^{+/+}$ and *ApoE*$^{-/-}$*Opg*$^{-/-}$ mice were categorized into three groups based on diameter and the presence of visible hematoma (No Aneurysm, Aneurysm, and Dissection groups). Scale bars indicate 1 mm. **(B)** External diameter of the SRA in AngII-infused *ApoE*$^{-/-}$*Opg*$^{+/+}$ (gray, n = 16) and *ApoE*$^{-/-}$*Opg*$^{-/-}$ (white, n = 16) mice. All measurements are shown as box plots and each measurement is shown as a white circle (No Aneurysm), gray triangle (Aneurysm), or black cross (Dissection). **(C)** The incidence (%) of aortic aneurysms is shown for No Aneurysm (white), Aneurysm (gray), and Dissection (black) groups. Statistical significance: p<0.05.

Dissection groups). In *ApoE*$^{-/-}$*Opg*$^{+/+}$ mice, 75% of SRAs were dilated and the majority of them had dissected (Fig 1C). However, in *ApoE*$^{-/-}$*Opg*$^{-/-}$ mice, 50% of SRAs were dilated and only a few had dissected. This suggests that Opg deficiency may have a preventive effect on AngII-induced aortic dilatation and dissection (43.75% in *ApoE*$^{-/-}$*Opg*$^{+/+}$ mice vs. 18.75% in *ApoE*$^{-/-}$*Opg*$^{-/-}$ mice).

Opg deficiency results in aneurysm with adventitial thickening

Since Opg deficiency may have a preventive effect on aortic dilatation and dissection, transverse cross-sections of the SRA were used to measure the size of the aortic lumen and evaluate the aortic wall structure, including the medial and adventitial layers. HE staining revealed narrower aortic lumens and smaller dissecting hematomas in *ApoE*$^{-/-}$*Opg*$^{-/-}$ mice compared to *ApoE*$^{-/-}$*Opg*$^{+/+}$ mice (Fig 2A(HE)). The area of the aortic internal lumen tended to be smaller in *ApoE*$^{-/-}$*Opg*$^{-/-}$ mice compared with *ApoE*$^{-/-}$*Opg*$^{+/+}$ mice, although the difference was not significant (Fig 2B).

There were no differences in the structure of medial elastic fibers in the Aneurysm group between *ApoE*$^{-/-}$*Opg*$^{-/-}$ and *ApoE*$^{-/-}$*Opg*$^{+/+}$ mice, as assessed by EVG and AZAN staining (Fig 2A (panels EVG and Aneurysm), S3A Fig in S1 File). In the Dissection group, a complete disappearance of medial elastic fibers in which atherosclerotic plaques invaded the disrupted side of the aortic circumference was observed in mice of both genotypes (Fig 2A (panels EVG and Aneurysm)). There was no significant difference in the width of the medial layer between mice
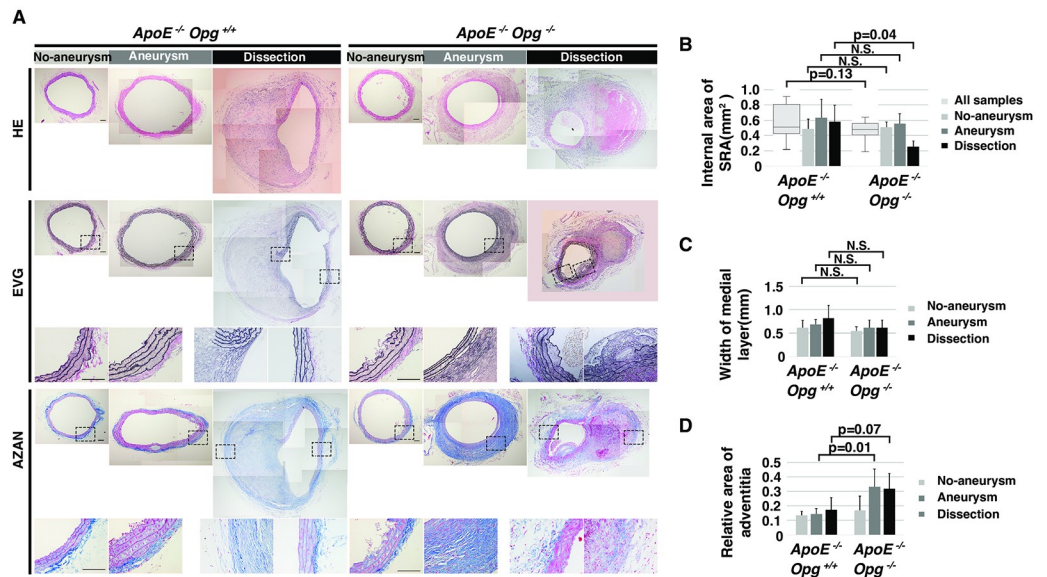
Fig 2. Opg deficiency tends to suppress AngII-induced aortic dilatation and promotes adventitial thickening. (A) Representative cross sections of the aorta stained with HE, EVG, and AZAN. Areas selected by boxes surrounded by a black dotted line are magnified below. Scale bars indicate 0.1 mm. **(B)** Internal area of the suprarenal aorta (SRA) of *ApoE^-/-^Opg^+/+^* (n = 16) and *ApoE^-/-^Opg^-/-^* (n = 16) mice. Measurements for all samples are presented as box plots. Measurements for the three groups are presented as bar graphs. n = 4 and 8 for the No-aneurysm group, n = 5 and 5 for the Aneurysm group, and n = 7 and 3 for the Dissection group in *ApoE^-/-^Opg^+/+^* and *ApoE^-/-^Opg^-/-^* mice, respectively. **(C)** Medial layer width of the SRA of AngII-infused mice in each group. N.S; not significant. **(D)** Relative adventitial area of the SRA of AngII-infused mice in each group. Statistical significance: p<0.05.

of both genotypes (Fig 2C). However, significant adventitial thickening and accumulation of collagen were noted in the Aneurysm and Dissection groups in *ApoE^-/-^Opg^-/-^* mice (Fig 2A (panel AZAN), Fig 2D, S3B Fig in S1 File). These observations suggest that adventitial thickening might be associated with the smaller aortic diameter and lower tendency of dissection in *ApoE^-/-^Opg^-/-^* mice.

Fibrotic remodeling of the SRA and accumulation of myofibroblasts in *ApoE^-/-^Opg^-/-^* mice

Given the accumulation of collagen in *ApoE^-/-^Opg^-/-^* mice, we examined the type of collagen that accumulated in the adventitia. Collagen I, but not collagen III, accumulated in *ApoE^-/-^Opg^-/-^* mice following AngII infusion (Fig 3A, S4A Fig and S4B Fig in S1 File). The area of collagen I expression was significantly larger in *ApoE^-/-^Opg^-/-^* mice compared to that in *ApoE^-/-^Opg^+/+^* mice (Fig 3B). As expected, no differences were found in collagen I expression between *ApoE^-/-^Opg^-/-^* and *ApoE^-/-^Opg^+/+^* mice in the H_2O-infused controls (S4C Fig in S1 File). Since TGF-β1 is the central mediator of fibrogenesis [22], we examined its mRNA expression in SRA tissue and found it to be significantly higher in *ApoE^-/-^Opg^-/-^* mice compared to *ApoE^-/-^Opg^+/+^* mice after AngII infusion (Fig 3C). This result further supports the finding that Opg deficiency promotes fibrotic remodeling of the aorta.

To determine the types of cells which accumulated in the adventitia, immunohistochemistry was performed using anti-SMA and anti-vimentin antibodies to mark smooth muscle cells and fibroblasts, respectively. In *ApoE^-/-^Opg^-/-^* mice, both SMA and vimentin were distributed in the adventitia, especially in the Aneurysm and Dissection groups (Fig 4A and 4B). Since both SMA and vimentin are known to be expressed in myofibroblasts, the accumulated cells
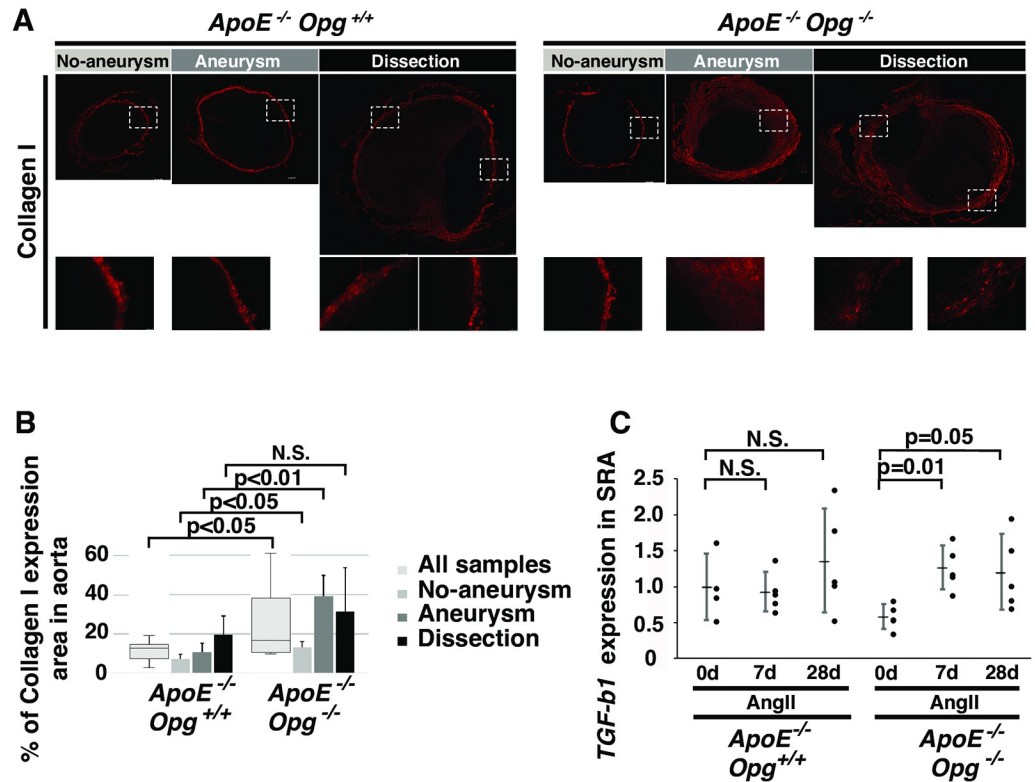
Fig 3. Collagen accumulation in aortas of *ApoE^{-/-}Opg^{-/-}* mice. (A) Representative immunofluorescence images of aortas of AngII-infused mice stained with an anti-collagen I antibody. Boxed areas (with white dotted lines) are magnified below. Scale bars indicate 100 μm. (B) Percent area of collagen I expression in aortas of *ApoE^{-/-}Opg^{+/+}* (n = 16) and *ApoE^{-/-}Opg^{-/-}* (n = 16) mice. Measurements for all samples are presented as box plots. Measurements for the three groups are presented as bar graphs (n = 4 and 8 for the No Aneurysm group, n = 5 and 5 for the Aneurysm group, and n = 7 and 3 for the Dissection group in *ApoE^{-/-}Opg^{+/+}* and *ApoE^{-/-}Opg^{-/-}* mice, respectively). (C) *Tgf-β1* mRNA expression in the SRA at days 0, 7, and 28 after initiation of AngII infusion in *ApoE^{-/-}Opg^{+/+}* (n = 4, 5, 5) and *ApoE^{-/-}Opg^{-/-}* (n = 5, 5, 5) mice. Statistical significance: $p < 0.05$.

that over-express collagen I in the adventitia of *ApoE^{-/-}Opg^{-/-}* mice are likely myofibroblasts. Interestingly, these myofibroblasts were found not only in the adventitia, but also in the outer layers of the media in *ApoE^{-/-}Opg^{-/-}* mice. Medial cells expressing SMA but not vimentin in *ApoE^{-/-}Opg^{+/+}* mice were unlikely to be myofibroblasts (Fig 4A). Next, we measured the expression of matrix metalloproteinases (MMPs) in SRA tissue, but found no difference between *ApoE^{-/-}Opg^{-/-}* and *ApoE^{-/-}Opg^{+/+}* mice after AngII infusion (S5A Fig-S5C Fig in S1 File). These findings collectively suggest that accumulation of myofibroblasts could be one of the causes of adventitial thickening in *ApoE^{-/-}Opg^{-/-}* mice after AngII infusion.

Up-regulation of Trail in SRAs of AngII-infused *ApoE^{-/-}Opg^{-/-}* mice

To understand how Opg deficiency contributes to adventitial thickening, we examined the expression of Trail in aneurysm tissue of AngII-infused *ApoE*-KO mice, given the known role of Opg as a decoy receptor for Trail [8]. Trail expression was up-regulated in the adventitia and outer layers of the media in *ApoE^{-/-}Opg^{-/-}* mice after AngII infusion (Fig 5A and 5C), but not in *ApoE^{-/-}Opg^{+/+}* mice or after H_2O infusion (S5D and S5F Fig in S1 File). Notably, Trail was mainly expressed in cells that were double positive for SMA and vimentin. These cells
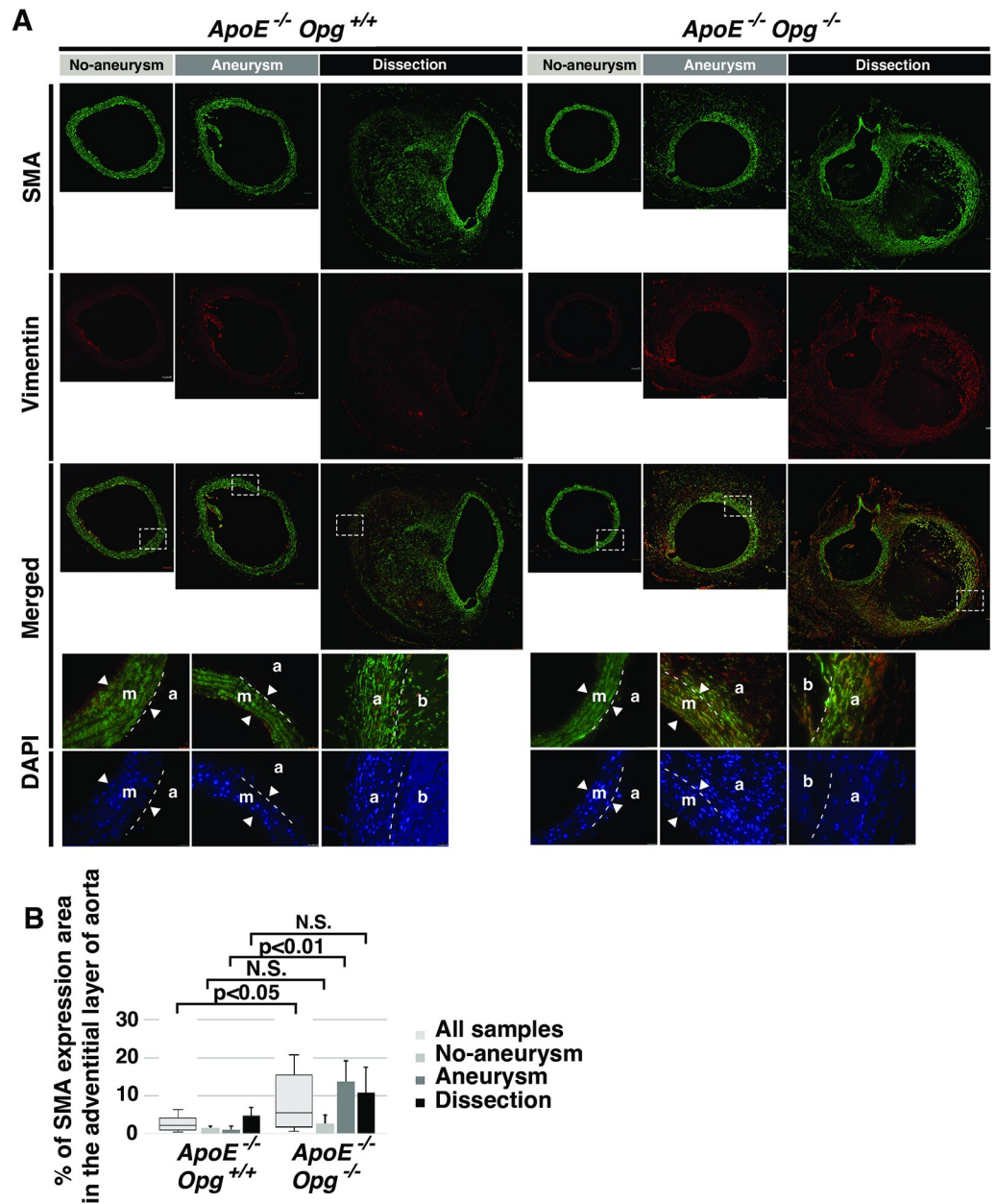
Fig 4. Accumulation of myofibroblasts in adventitias of AngII-infused *ApoE⁻/⁻Opg⁻/⁻* mice. (A) Representative double-immunofluorescence images of aortas after AngII infusion with anti- SMA (green) and anti-vimentin (red) antibodies. Scale bars indicate 100 μm. Areas selected by the white box (dotted line) are magnified below. Nuclei were stained with DAPI (blue). Scale bars indicate 25 μm. Medial layer (m), Adventitial layer (a), hematoma (b). The two arrowheads show borders of the medial layer. The white dotted line in the magnified panels indicates the border of the medial and adventitial layers. **(B)** Percent area of SMA expression in adventitias of *ApoE⁻/⁻Opg⁺/⁺* (n = 16) and *ApoE⁻/⁻Opg⁻/⁻* (n = 16) mice. Measurements for all samples are presented as box plots. Measurements for the three groups are presented as bar graphs. n = 4 and 8 for the No Aneurysm group, n = 5 and 5 for the Aneurysm group, and n = 7 and 3 for the Dissection group in *ApoE⁻/⁻Opg⁺/⁺* and *ApoE⁻/⁻Opg⁻/⁻* mice, respectively. Statistical significance: p<0.05.

https://doi.org/10.1371/journal.pone.0235553.g004

were also positive for Ki67, a cell proliferation marker (Fig 5B), implying that Trail induces the proliferation of these cells autonomously [23].

Trail has also been reported to promote chemotactic migration of not only SMCs, but also monocytes towards the site of inflammation [24]. Round shaped, F4/80 macrophages were
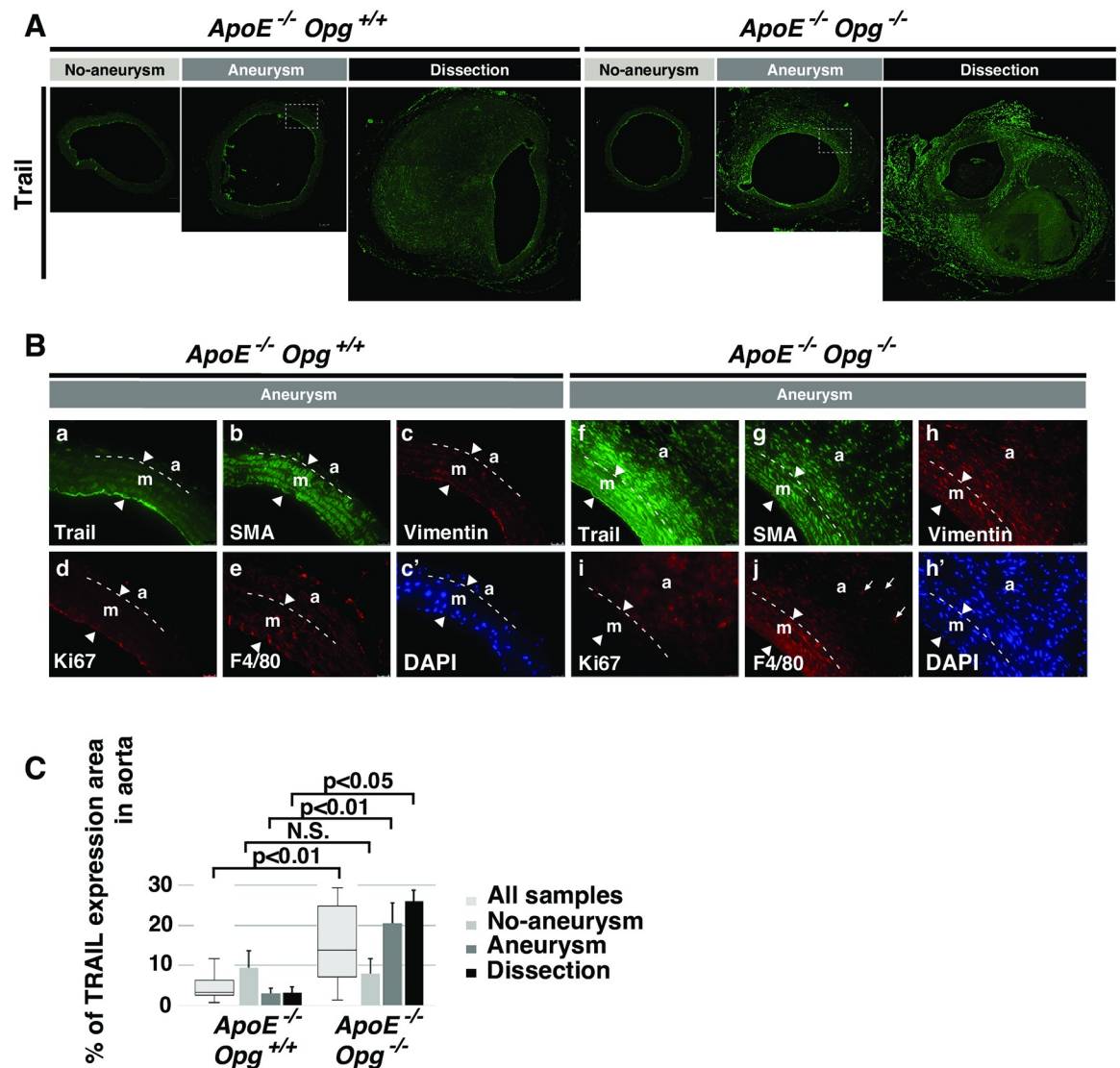
Fig 5. Trail upregulation in aneurysm tissue of AngII-infused *ApoE*^−/−^*Opg*^−/−^ mice. **(A)** Representative immunofluorescence images of aortic tissue sections from AngII-infused mice stained with anti-Trail (green) antibody. Scale bars indicate 100 μm. Areas selected by the white box (dotted line) in the Aneurysm group are magnified below. **(B)** Magnified immunofluorescence images of aortic tissue sections from the AngII-infused Aneurysm group stained with anti-Trail (green; a, f), anti-SMA (green; b, g), anti-vimentin (red; c, h), anti-Ki67 (red; d, i), and anti-F4/80 (red; e, j) antibodies in *ApoE*^−/−^*Opg*^+/+^ and *ApoE*^−/−^*Opg*^−/−^ mice. Nuclei were stained with DAPI (blue; c-DAPI, h-DAPI). Scale bars indicate 25 μm. Medial layer (m), adventitial layer (a). The two arrowheads show borders of the medial layer. The white dotted line in the magnified panels indicates the border of the medial and adventitial layers. Small arrows in panel j indicate large round-shaped macrophages infiltrating the adventitia. Statistical significance: p<0.05. **(C)** Percent area of Trail expression in medial and adventitial layers of *ApoE*^−/−^*Opg*^+/+^ (n = 16) and *ApoE*^−/−^*Opg*^−/−^ (n = 16) mice. Measurements for all samples are presented as box plots. Measurements for the three groups are presented as bar graphs. n = 4 and 8 for the No Aneurysm group, n = 5 and 5 for the Aneurysm group, and n = 7 and 3 for the Dissection group in *ApoE*^−/−^*Opg*^+/+^ and *ApoE*^−/−^*Opg*^−/−^ mice, respectively. Statistical significance: p<0.05.

detected in the adventitia of *ApoE*^−/−^*Opg*^−/−^ mice (Fig 5B; S5G Fig in S1 File), suggesting that increased Trail expression may lead to more inflammation, myofibroblast accumulation, and fibrotic remodeling of the aortic wall in Opg-deficient mice.

Discussion

Consistent with results reported by Moran et al. [19], we found that Opg deficiency tended to limit AngII-induced aortic dissection and dilatation. Gross phenotypic differences are evident

between the CaCl$_2$-induced aneurysm model and AngII-induced aneurysm model [18, 19]. However, we observed adventitial thickening accompanied by myofibroblast accumulation and increased expression of collagen I and Trail in aneurysm tissue of *ApoE$^{-/-}$Opg$^{-/-}$* mice. These pathological and cellular changes of the aortic wall were also reported in the CaCl$_2$-induced aneurysm model [18], suggesting that adventitial thickening with myofibroblast accumulation could be a common feature of Opg deficiency.

Myofibroblasts in aortic tissue promote the excessive production of extracellular matrix, including collagen, and subsequent fibrotic remodeling of the aorta [25]. Disorders of collagen fiber assembly are thought to underlie aortic dilatation and dissection. For example, weakness in connective tissue caused by mutations in various types of collagen and enzymes involved in collagen maturation in Ehlers-Danlos syndrome results in aortic aneurysms [26]. Moreover, Dobrin et al. reported that degradation of collagen, rather than elastin, is an important cause of aneurysm development, suggesting that collagen fibers protect the aorta from internal pressure-induced expansion [27]. When applied to the present study, these findings suggest that excessive collagen accumulation in the adventitia may have strengthened the aortic tissue. This in turn could have resulted in smaller aneurysms and a lower rate of dissection events in *ApoE$^{-/-}$Opg$^{-/-}$* mice in the AngII-induced aneurysm model. In light of studies reporting that Trail induces collagen I transcription in fibroblast cells [28], Trail could potentially play a role in collagen accumulation in myofibroblasts. Fibrotic remodeling of the aorta by myofibroblasts might protect against AngII-induced aneurysm and dissection in *ApoE$^{-/-}$Opg$^{-/-}$* mice.

In our previous study, which used the CaCl$_2$-induced aneurysm model, Opg deficiency exacerbated AAAs, despite adventitial thickening, increased Trail expression, and the appearance of myofibroblasts [18]. We speculate that the contrasting phenotypes of the AngII-induced and CaCl$_2$-induced aneurysm models could be due to different processes involved in aneurysm formation. In the AngII-induced *ApoE* KO mouse aneurysm model, local medial destruction is observed only in the plaque area. It is currently thought that aneurysms and dissection start at small cleavages which develop after infusion of AngII, leading to local destruction of the medial layer [29]. Concurrently, collagen accumulation in the adventitia induced by AngII infusion in *ApoE$^{-/-}$/Opg$^{-/-}$* mice limits the development of aneurysms and dissection. On the other hand, in the CaCl$_2$-induced model, complete destruction of the medial layer is observed in a broad area. This extensive destruction of the medial layer may promote enlargement of the aortic lumen. Increased Trail expression, due to the absence of Opg, up-regulates the expression of proteolytic enzymes, including Mmp9 and Mmp2, resulting in an acceleration of elastic medial tissue destruction. Although adventitial thickening simultaneously progresses after CaCl$_2$ treatment in *Opg* KO mice, it may be insufficient to compensate for the severe and extensive medial tissue destruction and limit aortic enlargement.

In conclusion, adventitial thickening with collagen accumulation induced by AngII infusion may increase the strength of aortic tissue and potentially limit the development of aortic aneurysms and dissection in *ApoE$^{-/-}$Opg$^{-/-}$* mice. At the same time, aortic tissue may lose flexibility in elastic vessels, thereby increasing cardiac load. AngII infusion in the absence of Opg may promote excessive reactions in aortic tissue, suggesting that Opg plays a potential role in aortic tissue homeostasis and maintenance of proper blood pressure. In the therapeutic context, targeting aortic tissue with agents that induce adventitial thickening with collagen accumulation may help suppress dissection events. Such treatments may include focal drug delivery systems in which an anti-Opg antibody is delivered to plaques, or direct application of drugs to stent grafts which would allow for focal induction of adventitial thickening.

Materials and methods

Mice

Opg KO (*ApoE*$^{+/+}$/*Opg*$^{-/-}$) mice of the C57BL/6J strain background (CLEA Japan, Inc.) were crossed with *ApoE* KO (*ApoE*$^{-/-}$/*Opg*$^{+/+}$) mice to obtain *ApoE*$^{+/-}$*Opg*$^{+/-}$ mice. Progeny were inter-crossed to establish an *ApoE*$^{-/-}$*Opg*$^{+/-}$ line, which was then inter-crossed to generate *ApoE*$^{-/-}$*Opg*$^{-/-}$ mice and control *ApoE*$^{-/-}$*Opg*$^{+/+}$mice. Genotypes were determined by PCR (94˚C for 30 sec; 55˚C for 30 sec and 72˚C for 30 sec for 35 cycles) using the following primers: forward primer 5'-CTG ACC ACT CTT ATA CGG AC AG-3' and reverse primer 5'-CTA AGT TAG CTG CTG TCT GGC-3' for the *Opg*-wild type allele; forward primer 5'-CTG ACC GCT TCC TCG TGC TTTAC-3' and the above-mentioned reverse primer for the *Opg*-mutant allele; forward primer 5'-ACT CTA CAC AGG ATG CCT AGC-3' and reverse primer 5'-CTC ACG TCA GTT CTT GTG TGAC-3' for the *ApoE*-wild type allele; and the above-mentioned forward primer and reverse primer 5'-GCC GCC CGA CTG CAT CT-3' for the *ApoE*-mutant allele.

Aortic aneurysm model

Six-month-old male *ApoE*$^{-/-}$*Opg*$^{+/+}$ (n = 16) and *ApoE*$^{-/-}$*Opg*$^{-/-}$ (n = 16) mice were infused with AngII as described previously [30]. Under anesthesia, a micro-osmotic pump (ALZET Model 1004, Durect Corporation) was implanted into the subcutaneous space left of the dorsal midline for infusion of AngII (Sigma-Aldrich) or H_2O at a rate of 1.0 μg/kg/min for 28 days. Mice were sacrificed by anesthetia overdose. After cutting the sternum and exposing the thoracic cavity, blood from the right ventricle was collected for storage during perfusion with PBS. Mice were then perfused with 4% paraformaldehyde. Whole aortas were excised for morphometric analysis and measurement of SRA diameters. Images were taken of whole aortas to measure the external diameter of SRAs. SRAs were then separated from aortas and embedded in paraffin for subsequent histological analysis.

For RNA isolation, aortas were harvested after perfusion with PBS and stored in RNA-later solution (Ambion). This experiment was approved by the Committee of Animal Experimentation at Hiroshima University (A08-32) and carried out in accordance with the approved protocol. All surgeries were performed under a combination of three anesthetic solutions (medetomidine, butorphanol, and midazolam), and efforts were made to minimize suffering during and after surgery.

Morphological examination and measurement of aortic diameters

The maximum external diameter of the SRA as shown in S1A Fig in S1 File was measured (Fig 1B). The external diameter of the SRA in the H_2O-infused group (S2C Fig in S1 File) was used as a control to categorize AngII-infused aortas into three groups based on maximum external diameter and the presence of visible hematoma (No-aneurysm group: diameter less than 1.5 times the H_2O-infused control; Aneurysm group: diameter more than 1.5 times the H_2O-infused control without visible hematoma; Dissection group: diameter more than 1.5 times the H_2O-infused control with visible hematoma). Paraffin-embedded aortic tissues were used to generate 6 μm-thick sections, which were cut at the level of the SRA. The tissue sections were then subjected to Hematoxylin/Eosin (HE), Elastica van Gieson (EVG), and Analine Blue (AZAN) staining. The sections were used to measure the internal area of the SRA, the width of the medial layer, and the relative area of the adventitia. Borders of the aortic lumen were marked with a dotted circle (S1B Fig in S1 File) and used to measure the internal area of the SRA (Fig 2B). Red lines show 5–8 measurements of the medial layer width on the side of the

aortic circumference which was not disrupted by atherosclerotic plaques (S1B Fig in S1 File). Average values were used (Fig 2C). The total area (TA) of the aorta included all aortic layers. The arterial area (AA), which included the lumen, endothelium, and media, and the bleeding area (BA), which included hematoma between medial and adventitial layers, were marked by dotted circles (S1C Fig and S1D Fig in S1 File). After measuring each area, the relative area of the adventitia was calculated using the following equation: TA-AA-BA/TA. The % area of collagen I expression was calculated by dividing the signal area by the entire aortic area (excluding the hematoma area) (Fig 3B). The % area of SMA expression was calculated by dividing the signal area by the area of the adventitial layer (Fig 4B). The % area of Trail expression was calculated by dividing the signal area by the area of medial and adventitial layers (Fig 5C). Area selection was performed using Photoshop software and was confirmed by three independent researchers. Area measurements were performed using Image-J software (NIH, USA).

Immunohistochemistry (IHC)

Sections were pre-incubated in antigen retrieval solution (pH 5.2) at 90˚C for 45 minutes, based on the manufacturer's instructions (Dako), and then blocked with 1% bovine serum albumin in 0.1% Tween-phosphate buffered solution (PBS) for 1 hr. After pre-treatment and blocking, sections were incubated with a primary antibody overnight at 4˚C and subsequently with appropriate secondary antibodies for 2 hr at room temperature, followed by counterstaining with 4'-6-diamidino-2-phenylindole (DAPI). After primary antibodies, listed in Table 1, sections were treated with anti-mouse, -rat, or -rabbit antibodies conjugated wiith Alexa Fluor 488 or 555 dye (donkey, 1:500; Life Technologies). Signals were detected using a DMI4000 fluorescence microscope (Leica Microsystems).

Quantitative Real-time PCR

Total RNA was isolated using TRIzol reagent (Invitrogen). Reverse transcription was performed using the ReverTra Ace qPCR RT Kit (TOYOBO). Real-time PCR was conducted using SYBR Premix Ex Taq II (Takara Bio Inc. and Kapa Biosystems Inc.). Intensities of PCR products using primers, listed in Table 2, were measured and analyzed using Opticon (MJ Research). Amplification conditions were as follows: 5 s at 95˚C, 20 s at 60˚C, and 15 s at 72˚C for 49 cycles. *G3pdh* was used as the internal control.

Serum cholesterol measurement

Concentrations of serum cholesterol were measured in $ApoE^{-/-}Opg^{+/+}$ and $ApoE^{-/-}Opg^{-/-}$ mice on days 0, 7, and 28 after initiation of AngII infusion. Measurements were performed by JaICA, Nikken Seil Co., Ltd (Shizuoka, Japan).

Table 1. List of antibodies.

Specificity	Vendor	Cat#	Lot#	dilution
Collagen I	Abcam	ab21286	GR46228-1	1:250
Collagen III	Abcam	ab7778	GR52659-1	1:250
TRAIL	Abcam	ab2435	GR14018-5	1:50
Actin, α-Smooth Muscle (Monoclonal clone 1A4)	Sigma-Aldrich	A2547	032M4822	1:200
Vimentin	BioVision	3634		1:50
Ki67	Abcam	ab15580	GR101835-1	1:100
F4/80 (BM8)	Santa Cruz	sc-52664	B1810	1:50

https://doi.org/10.1371/journal.pone.0235553.t001

Table 2. List of PCR primers.

Genes	Sequences	Product size (bp)
Mmp-9:	forward 5' -GCCCTGGAACTCACACGACA-3'	85
	reverse 5'-TTGGAAACTCACACGCCAGAAG-3'	
Mmp-2:	forward 5'-CTCCTACAACAGCTGTACCAC-3'	182
	reverse 5'-CATACTTGTTGCCCAGGAAAG-3'	
Tgf-β1:	forward 5'- ATCGACATGGAGCTGGTGAAA-3'	76
	reverse 5'- TGGCGAGCCTTAGTTTGGA-3'	
G3pdh:	forward 5'- ACCACAGTCCATGCCATCAC-3'	452
	reverse 5'- TCCACCACCCTGTTGCTGTA-3'	

Statistical analysis

Non-parametric analyses, including the Mann-Whitney U-test or Kruskal-Wallis test with Scheffe's and Steel-Dwass post hoc analyses, and ordinal logistic regression analyses were conducted using Ekuseru-Toukei 2012 software (Social Survey Research Information Co., Ltd.). Data are expressed as mean ± standard deviation (SD). $P < 0.05$ was considered statistically significant.

Supporting information

S1 File.
(PDF)

Author Contributions

Conceptualization: Batmunkh Bumdelger, Chiemi Sakai, Mari Ishida, Hiroki Kokubo, Masao Yoshizumi.

Funding acquisition: Masao Yoshizumi.

Investigation: Batmunkh Bumdelger, Mikage Otani, Kohei Karasaki.

Methodology: Batmunkh Bumdelger, Hiroki Kokubo.

Project administration: Batmunkh Bumdelger, Hiroki Kokubo.

Supervision: Hiroki Kokubo, Masao Yoshizumi.

Validation: Chiemi Sakai, Mari Ishida, Masao Yoshizumi.

Writing – original draft: Batmunkh Bumdelger, Mikage Otani, Kohei Karasaki.

Writing – review & editing: Mikage Otani, Kohei Karasaki, Hiroki Kokubo, Masao Yoshizumi.

References

1. Golledge J, Norman PE. Atherosclerosis and abdominal aortic aneurysm: cause, response, or common risk factors? Arterioscler Thromb Vasc Biol. 2010; 30(6):1075–7. https://doi.org/10.1161/ATVBAHA.110.206573 PMID: 20484703

2. Daugherty A, Cassis LA. Mouse models of abdominal aortic aneurysms. Arteriosclerosis, thrombosis, and vascular biology. 2004; 24(3):429–34. https://doi.org/10.1161/01.ATV.0000118013.72016.ea PMID: 14739119.

3. Patelis N, Moris D, Schizas D, Damaskos C, Perrea D, Bakoyiannis C, et al. Animal models in the research of abdominal aortic aneurysms development. Physiological research. 2017; 66(6):899–915. https://doi.org/10.33549/physiolres.933579 PMID: 28937252.

4. Ailawadi G, Eliason JL, Upchurch GR Jr. Current concepts in the pathogenesis of abdominal aortic aneurysm. J Vasc Surg. 2003; 38(3):584–8. Epub 2003/08/30. https://doi.org/10.1016/s0741-5214(03)00324-0 PMID: 12947280.

5. Longo GM, Xiong W, Greiner TC, Zhao Y, Fiotti N, Baxter BT. Matrix metalloproteinases 2 and 9 work in concert to produce aortic aneurysms. J Clin Invest. 2002; 110(5):625–32. Epub 2002/09/05. https://doi.org/10.1172/JCI15334 PMID: 12208863.

6. Annambhotla S, Bourgeois S, Wang X, Lin PH, Yao Q, Chen C. Recent advances in molecular mechanisms of abdominal aortic aneurysm formation. World journal of surgery. 2008; 32(6):976–86. https://doi.org/10.1007/s00268-007-9456-x PMID: 18259804

7. Golledge J, Muller J, Daugherty A, Norman P. Abdominal aortic aneurysm: pathogenesis and implications for management. Arterioscler Thromb Vasc Biol. 2006; 26(12):2605–13. https://doi.org/10.1161/01.ATV.0000245819.32762.cb PMID: 16973970.

8. Baud'huin M, Duplomb L, Teletchea S, Lamoureux F, Ruiz-Velasco C, Maillasson M, et al. Osteoprotegerin: multiple partners for multiple functions. Cytokine Growth Factor Rev. 2013; 24(5):401–9. https://doi.org/10.1016/j.cytogfr.2013.06.001 PMID: 23827649.

9. Simonet WS, Lacey DL, Dunstan CR, Kelley M, Chang MS, Luthy R, et al. Osteoprotegerin: a novel secreted protein involved in the regulation of bone density. Cell. 1997; 89(2):309–19. https://doi.org/10.1016/s0092-8674(00)80209-3 PMID: 9108485.

10. Tsuda E, Goto M, Mochizuki S, Yano K, Kobayashi F, Morinaga T, et al. Isolation of a novel cytokine from human fibroblasts that specifically inhibits osteoclastogenesis. Biochem Biophys Res Commun. 1997; 234(1):137–42. Epub 1997/05/08. https://doi.org/10.1006/bbrc.1997.6603 PMID: 9168977.

11. Bucay N, Sarosi I, Dunstan CR, Morony S, Tarpley J, Capparelli C, et al. Osteoprotegerin-deficient mice develop early onset osteoporosis and arterial calcification. Genes & development. 1998; 12 (9):1260–8. https://doi.org/10.1101/gad.12.9.1260 PMID: 9573043

12. Sattler AM, Schoppet M, Schaefer JR, Hofbauer LC. Novel aspects on RANK ligand and osteoprotegerin in osteoporosis and vascular disease. Calcified tissue international. 2004; 74(1):103–6. https://doi.org/10.1007/s00223-003-0011-y PMID: 14523602.

13. Zhang J, Fu M, Myles D, Zhu X, Du J, Cao X, et al. PDGF induces osteoprotegerin expression in vascular smooth muscle cells by multiple signal pathways. FEBS Lett. 2002; 521(1–3):180–4. Epub 2002/06/18. https://doi.org/10.1016/s0014-5793(02)02872-7 PMID: 12067713.

14. Jono S, Otsuki S, Higashikuni Y, Shioi A, Mori K, Hara K, et al. Serum osteoprotegerin levels and long-term prognosis in subjects with stable coronary artery disease. J Thromb Haemost. 2010; 8(6):1170–5. https://doi.org/10.1111/j.1538-7836.2010.03833.x PMID: 20230427.

15. Schoppet M, Sattler AM, Schaefer JR, Herzum M, Maisch B, Hofbauer LC. Increased osteoprotegerin serum levels in men with coronary artery disease. The Journal of clinical endocrinology and metabolism. 2003; 88(3):1024–8. https://doi.org/10.1210/jc.2002-020775 PMID: 12629080.

16. Moran CS, McCann M, Karan M, Norman P, Ketheesan N, Golledge J. Association of osteoprotegerin with human abdominal aortic aneurysm progression. Circulation. 2005; 111(23):3119–25. Epub 2005/06/09. CIRCULATIONAHA. https://doi.org/10.1161/CIRCULATIONAHA.104.464727 PMID: 15939823.

17. Koole D, Hurks R, Schoneveld A, Vink A, Golledge J, Moran CS, et al. Osteoprotegerin is associated with aneurysm diameter and proteolysis in abdominal aortic aneurysm disease. Arterioscler Thromb Vasc Biol. 2012; 32(6):1497–504. Epub 2012/04/21. https://doi.org/10.1161/ATVBAHA.111.243592 PMID: 22516062.

18. Bumdelger B, Kokubo H, Kamata R, Fujii M, Yoshimura K, Aoki H, et al. Osteoprotegerin Prevents Development of Abdominal Aortic Aneurysms. PLoS one. 2016; 11(1):e0147088. https://doi.org/10.1371/journal.pone.0147088 PMID: 26783750.

19. Moran CS, Jose RJ, Biros E, Golledge J. Osteoprotegerin Deficiency Limits Angiotensin II-Induced Aortic Dilatation and Rupture in the Apolipoprotein E-Knockout Mouse. Arteriosclerosis, thrombosis, and

vascular biology. 2014; 34(12):2609–16. https://doi.org/10.1161/ATVBAHA.114.304587 PMID: 25301844

20. Vorkapic E, Kunath A, Wagsater D. Effects of osteoprotegerin/TNFRSF11B in two models of abdominal aortic aneurysms. Molecular medicine reports. 2018; 18(1):41–8. https://doi.org/10.3892/mmr.2018. 8936 PMID: 29749489

21. Daugherty A, Manning MW, Cassis LA. Antagonism of AT2 receptors augments angiotensin II-induced abdominal aortic aneurysms and atherosclerosis. Br J Pharmacol. 2001; 134(4):865–70. Epub 2001/10/19. https://doi.org/10.1038/sj.bjp.0704331 PMID: 11606327.

22. Biernacka A, Dobaczewski M, Frangogiannis NG. TGF-beta signaling in fibrosis. Growth Factors. 29(5):196–202. Epub 2011/07/12. https://doi.org/10.3109/08977194.2011.595714 PMID: 21740331.

23. Kavurma MM, Schoppet M, Bobryshev YV, Khachigian LM, Bennett MR. TRAIL stimulates proliferation of vascular smooth muscle cells via activation of NF-kappaB and induction of insulin-like growth factor-1 receptor. J Biol Chem. 2008; 283(12):7754–62. Epub 2008/01/08. https://doi.org/10.1074/jbc. M706927200 PMID: 18178561.

24. Wei W, Wang D, Shi J, Xiang Y, Zhang Y, Liu S, et al. Tumor necrosis factor (TNF)-related apoptosis-inducing ligand (TRAIL) induces chemotactic migration of monocytes via a death receptor 4-mediated RhoGTPase pathway. Mol Immunol. 47(15):2475–84. Epub 2010/07/20. https://doi.org/10.1016/j. molimm.2010.06.004 PMID: 20638129.

25. Leask A. Potential therapeutic targets for cardiac fibrosis: TGFbeta, angiotensin, endothelin, CCN2, and PDGF, partners in fibroblast activation. Circ Res. 2010; 106(11):1675–80. https://doi.org/10.1161/ CIRCRESAHA.110.217737 PMID: 20538689.

26. Malfait F. Vascular aspects of the Ehlers-Danlos Syndromes. Matrix biology: journal of the International Society for Matrix Biology. 2018; 71–72:380–95. https://doi.org/10.1016/j.matbio.2018.04.013 PMID: 29709596.

27. Dobrin PB, Mrkvicka R. Failure of elastin or collagen as possible critical connective tissue alterations underlying aneurysmal dilatation. Cardiovasc Surg. 1994; 2(4):484–8. Epub 1994/08/01. PMID: 7953454.

28. Yurovsky VV. Tumor necrosis factor-related apoptosis-inducing ligand enhances collagen production by human lung fibroblasts. Am J Respir Cell Mol Biol. 2003; 28(2):225–31. Epub 2003/01/24. https://doi. org/10.1165/rcmb.2002-0140OC PMID: 12540490.

29. Trachet B, Aslanidou L, Piersigilli A, Fraga-Silva RA, Sordet-Dessimoz J, Villanueva-Perez P, et al. Angiotensin II infusion into ApoE-/- mice: a model for aortic dissection rather than abdominal aortic aneurysm? Cardiovascular research. 2017; 113(10):1230–42. https://doi.org/10.1093/cvr/cvx128 PMID: 28898997.

30. Lederle FA. The natural history of abdominal aortic aneurysm. Acta Chir Belg. 2009; 109(1):7–12. Epub 2009/04/04. https://doi.org/10.1080/00015458.2009.11680364 PMID: 19341189.